Effects of mesh deformation on the accuracy of mixed finite element approximations for 3D Darcy's flows

Philippe R B Devloo, Omar Duran, Agnaldo M Farias, Sonia M. Gomes

Effects of mesh deformation on the accuracy of mixed finite element approximations for 3D Darcy's flows

Philippe R. B. Devloo[1], Omar Durán[2], Agnaldo M. Farias [3], and Sônia M. Gomes [4]

September 24, 2018

Abstract

H(div)-conforming finite element approximation spaces are usually formed by locally backtracking vector polynomial spaces defined on the master element by the Piola transformation. The main focus of the present paper is to study the effect of using non-affine elements on the accuracy of three dimensional flux approximations based on such spaces. For instance, instead of order $k+1$ for flux and flux divergence obtained with Raviart-Thomas or Nédélec spaces with normal fluxes of degree k, based on affine hexahedra or triangular prisms, reduced orders k for flux and $k-1$ for flux divergence may occur for distorted elements. To improve this scenario, a hierarchy of enriched flux approximations is considered, with increasing orders of divergence accuracy, holding for general space stable configurations. The original vector polynomial space is required to be expressed by a decomposition in terms of edge and internal shape functions. The enriched versions are defined by adding internal shape functions of the original family of spaces up to higher degree level $k+n$, $n>0$, while keeping fixed the original border fluxes of degree k. This procedure gives approximations with the same original flux accuracy, but with enhanced divergence order $k+n+1$, in the affine case, or $k+n-1$ for elements mapped by general multi-linear mappings. The loss of convergence in the flux variable due to quadrilateral face distortions cannot be corrected by including higher order internal functions. Application of these enriched flux spaces to the mixed finite element formulation of a Darcy's model problem is discussed. The computational cost of matrix assembly increases with n, but the global condensed systems to be solved have same dimension and structure of the original scheme.

[1]FEC-Universidade Estadual de Campinas, Campinas-SP, Brazil, phil@fec.unicamp.br

[2]FEC-Universidade Estadual de Campinas, Campinas-SP, Brazil, oduran@unicamp.br

[3]Departamento de Matemática, IFNMG, Salinas, MG, Brazil, agnaldo.farias@ifnmg.edu.br

[4]IMECC-Universidade Estadual de Campinas, Campinas, SP, Brazil, soniag@ime.unicamp.br

1 Introduction

The mixed finite element formulation for elliptic problems is attractive for the simulation of fluid flow and transport, as they provide accurate and locally mass conservative velocity fields, and handle well discontinuous coefficients. The method requires balanced pairs of approximation spaces $U_h \subset L^2(\Omega)$ and $\mathbf{V}_h \subset \mathbf{H}(\mathrm{div}, \Omega)$, for potential and flux variables, respectively. They are piecewise formed by local spaces $U(K)$ and $\mathbf{V}(K)$, over the elements K of partitions $\mathcal{T}_h = \{K\}$ of the computational domain Ω, which are obtained backtracking scalar $\hat{U}$ and vector $\hat{\mathbf{V}}$ polynomial spaces, defined on the master element $\hat{K}$. Usual transformations are used for scalar fields, but Piola transformations are required in order to keep the $\mathbf{H}(\mathrm{div})$-conformity of the mapped vector fields [1].

When affine geometric meshes are used, the kind of vector polynomial functions in $\hat{U}$ and $\hat{\mathbf{V}}$ are preserved in $U(K)$ and $\mathbf{V}(K)$. Otherwise, the functions in $U(K)$ and $\mathbf{V}(K)$ may not be polynomials anymore, and accuracy degradation may occur, specially for the vector fields. This fact is important in applications, for instance, to geological media, such as in aquifers or petroleum reservoirs, for which distorted meshes for irregular domains are usually required, as illustrated in [2]. Because of this drawback, the technique has to be used with special care in such cases, specially for low order schemes.

The present article studies some effects on the accuracy of the approximated variables in mixed formulations that can be caused by the use of non-affine hexahedral or prismatic meshes. For instance, instead of order $k+1$ for flux, potential and flux divergence approximations reached by the Nédélec-Raviart-Thomas spaces [3] (here denoted by RT_k) based on affine hexahedra, or by Nédélec N_k spaces for affine prisms [4], these orders may be reduced to k, for the flux, and to $k-1$, for the flux divergence, if the elements are mapped by general tri-linear or bi-linear mappings, respectively, causing degeneration of the quadrilateral faces of the elements.

As shall be clarified latter in the paper, accuracy degradation occurs due to the fact that, after the application of Piola transformations associated to such deformed elements, the only guarantee is that vector polynomials of total degree $k-1$ can be represented in the corresponding flux approximation spaces, and that the divergence of them contains polynomials of total degree $k-2$. On this subject, the study in [5] characterizes optimal properties to be held by a reference vector polynomial space $\hat{\mathbf{V}}$ such that a desired convergence rate by approximations in the resulting spaces $\mathbf{V}(K)$ is guaranteed after the action of the Piola tranformation associated to such kind of hexahedral or prismatic deformed elements K.

In order to improve the above mentioned approximation scenarios, enhanced versions of them shall be considered. In both cases, enriched flux spaces $\hat{\mathbf{V}}^+$ are created by adding to their original reference space $\hat{\mathbf{V}}$ some properly chosen internal functions (with zero normal components on the faces) of degree $k+2$, having divergence matching the corresponding potential functions $\hat{U}^+ = \hat{U}_{k+1}$ (with higher degree than the border fluxes, which are kept at degree k). These kind of stable enriched spaces have been considered for affine meshes in [6], where

hierarchical shape functions are constructed for them. As shall be proved in Section 6, this enrichment procedure is sufficient to produce mixed formulations with improved flux divergence accuracy, going from the reduced order $k-1$ of the original scheme to order k, matching the flux accuracy order, which is kept the same by the enriched configurations. Potential accuracy is also maintained at the original order $k+1$.

Pushing forward the frontier of this research area, the present paper also addresses the following contributions:

- As remarked in [7], for two-dimensional triangular and quadrilateral meshes, the enrichment methodology can also be applied to other existing stable space configurations $\{\hat{\mathbf{V}}_k, \hat{U}_k\}$ for the mixed method, k indicating the polynomial degree of flux face functions, in order to get an enriched version $\{\hat{\mathbf{V}}_k^+, \hat{U}_k^+\}$, provided some mild conditions are verified by the original space framework. Consequently, from a space configuration of type $\{\hat{\mathbf{V}}_k^+,\ \hat{U}_k^+\}$, we can imagine a new enhanced configuration $\{\hat{\mathbf{V}}_k^{++},\ \hat{U}_k^{++}\}$, and so on. We shall consider stable super-enhanced space configurations $\{\hat{\mathbf{V}}_k^{n+},\ \hat{U}_k^{n+}\}$, $n \geq 1$, which can hold without any geometry or dimension constraint.

- Another goal is to verify to which extent previous error analyses developed for the mixed method with approximation spaces based on non-affine quadrilateral elements, mapped by general bi-linear transformations (e.g. in [8, 9, 7]), can be generalized to consider the proposed enriched space configurations based on non-affine hexahedral and prismatic elements mapped by general tri-linear or bi-linear maps, respectively. For such deformed element cases, the conclusion is that divergence errors can be obtained with arbitrary high orders with the enriched spaces of type $\{\hat{\mathbf{V}}_k^{n+},\ \hat{U}_k^{n+}\}$, for increasing n. However, flux errors may not be improved, staying at the same order of the corresponding original versions. Furthermore, since the best convergence rate that can be observed for potential fields is one unit more than for the flux errors, they do not improve as well.

The paper is organized as follows. General aspects on notation for element geometries, polynomial spaces, transformations, and approximation spaces are set in Section 2. A summary of some aspects about mixed element formulation for an elliptic model problem is presented in Section 3, for which a general error analysis script is established. The proposed enriched approximation space configurations are described in Section 4, where an error analysis is performed by identifying the principal hypotheses required by the general script of Section 3. Three specific examples of enriched versions $\{\hat{\mathbf{V}}_k^{n+},\ \hat{U}_k^{n+}\}$, $n \geq 1$, are discussed in Section 5, for tetrahedral, hexahedral and prismatic meshes. Section 6 contains some results verifying the a priori estimates of previous sections, and Section 7 gives the final conclusions.

2 Notation and general aspects

2.1 Geometry

For the present study, the considered master elements are:

- Tetrahedron: $\hat{K} = \mathcal{T}_e = \{(\hat{x}, \hat{y}, \hat{z}); \hat{x} \geq 0, \hat{y} \geq 0, \hat{z} \geq 0, \hat{x} + \hat{y} + \hat{z} \leq 1\}$.
- Hexahedron: $\hat{K} = \mathcal{H}_e = [-1, 1] \times [-1, 1] \times [-1, 1]$.
- Prism: $\hat{K} = \mathcal{P}_r = \mathcal{T} \times [0, 1]$, where $\mathcal{T} = \{(\hat{x}, \hat{y}); \hat{x} \geq 0, \hat{y} \geq 0, \hat{x} + \hat{y} \leq 1\}$.

2.2 Polynomial spaces

Approximation spaces are defined backtracking polynomial spaces defined on the master elements. The following types of polynomials shall be used:

- $\mathbb{Q}_{l,m,n} = span\{x^i y^j z^k; i \leq l, j \leq m, k \leq n\}$ is the scalar polynomial space of maximum degree l in x, m in y, and n in z (used for hexahedral elements). Similar spaces for quadrilaterals faces are denoted by $\mathbb{Q}_{l,m}$.
- $\mathbb{P}_k = span\{x^i y^j z^k; i + j + k \leq k\}$, is the scalar polynomial space of total degree k (used for tetrahedral elements). The same notation is used for polynomials of total degree k on triangular faces.
- $\mathbb{W}_{m,n} = span\{x^i y^j z^k; i + j \leq m, k \leq n\}$ (used for prisms).

2.3 Transformations

Let $\Omega \subset \mathbb{R}^3$ be a computational region covered by a regular partition $\mathcal{T}_h = \{K\}$, where h refers to the maximum element diameter. For each geometric element $K \in \mathcal{T}_h$ there is an associated master element $\hat{K}$ and an invertible geometric diffeomorfism $F_K : \hat{K} \to K$ transforming $\hat{K}$ onto K. The geometric transformations considered in this study are of the form:

- Affine transformations: $F_K(\hat{x}, \hat{y}, \hat{z}) = A_0 + A_1\hat{x} + A_2\hat{y} + A_3\hat{z}$.
- Non-affine bi-linear (used for general prisms) or tri-linear transformations (used for general hexahedra):

$$\begin{aligned} F_K(\hat{x}, \hat{y}, \hat{z}) &= A_0 + A_1\hat{x} + A_2\hat{y} + A_3\hat{z} + C_1\hat{x}\hat{z} + C_2\hat{y}\hat{z}, \\ F_K(\hat{x}, \hat{y}, \hat{z}) &= A_0 + A_1\hat{x} + A_2\hat{y} + A_3\hat{z} + C_1\hat{x}\hat{y} + C_2\hat{x}\hat{z} + C_3\hat{y}\hat{z} + D\hat{x}\hat{y}\hat{z}. \end{aligned}$$

The coefficients A_i, C_i and D are constant vectors in $\mathbb{R}^3$.

2.4 Approximation spaces

Based on partitions $\mathcal{T}_h$ of the computational region, finite dimensional approximation spaces $\mathbf{V}_h \subset \mathbf{H}(\mathrm{div}, \Omega)$ and $U_h \subset L^2(\Omega)$ are piecewise defined over the elements K. Different contexts shall be considered for any element geometry, all sharing the following basic characteristics.

1. A vector polynomial space $\hat{\mathbf{V}}$ and a scalar polynomial space $\hat{U}$ are considered on the master element $\hat{K}$.

2. In all the cases, the divergence operator maps $\hat{\mathbf{V}}$ onto $\hat{U}$:

$$\nabla \cdot \hat{\mathbf{V}} = \hat{U}. \tag{1}$$

3. $\hat{\mathbf{V}}$ is spanned by a hierarchy of vector shape functions organized into two classes: the shape functions of interior type, with vanishing normal components over all element faces, and the shape functions associated to the element faces, otherwise. Thus, a direct decomposition $\hat{\mathbf{V}} = \hat{\mathbf{V}}^{\partial} \oplus \mathring{\hat{\mathbf{V}}}$, in terms of face and internal flux functions, naturally holds.

4. The functions $\mathbf{q} \in \mathbf{V}_h$ and $\varphi \in U_h$ are piecewise defined: $\mathbf{q}|_K \in \mathbf{V}(K)$ and $\varphi|_K \in U(K)$, by locally backtracking the polynomial spaces $\hat{\mathbf{V}}$ and $\hat{U}$. The Piola transformation $\mathbb{F}_K^{\mathrm{div}}$ or the usual mapping of scalar functions $\mathbb{F}_K$ are used, both induced by the diffeomorfism F_K. Precisely:

   - Vector functions defined in K are set as

   $$\mathbf{V}(K) = \mathbb{F}_K^{div}\hat{\mathbf{V}} = \left\{\mathbf{q}|\ J_K\ DF_K^{-1}\mathbf{q} \circ \mathbb{F}_K \in \hat{\mathbf{V}}\right\},$$

   where DF_K is the Jacobian matrix of F_K, and $J_K = det(DF_K)$. It is assumed that $J_K > 0$. It can be verified that for $\hat{\mathbf{q}} \in \hat{\mathbf{V}}$, and $\hat{\mathbf{x}} \in \hat{K}$

   $$\nabla \cdot \hat{\mathbf{q}} = J_K(\hat{\mathbf{x}})\nabla \cdot \mathbf{q}. \tag{2}$$

   - Scalar functions defined in K are given by

   $$U(K) = \mathbb{F}_K\hat{U} = \left\{\varphi|\ \varphi \circ \mathbb{F}_K \in \hat{U}\right\}.$$

The construction of hierarchic shape functions $\hat{\mathbf{\Phi}}$ is described in [10] for some classic vector spaces $\hat{\mathbf{V}}$ based on triangle (BDM_k [11] and $BDFM_k$ [12]) and quadrilateral (RT_k) master elements. It is based on appropriate choice of constant vector fields $\hat{\mathbf{v}}$, based on the geometry of each master element, which are multiplied by an available set of H^1 hierarchical scalar basis functions $\hat{\varphi}$ to get $\hat{\mathbf{\Phi}} = \hat{\mathbf{v}}\hat{\varphi}$. There are shape functions of interior type, with vanishing normal components over all element edges. Otherwise, the shape functions are classified of edge type. The normal component of an edge function coincides on the corresponding edge with the associated scalar shape function, and vanishes

over the other edges. The required set of H^1 hierarchical scalar basis functions are the ones constructed in [13].

Particularly, the resulting flux spaces $\hat{\mathbf{V}}$ are spanned by bases $\hat{\mathbf{B}}$ of the form

$$\hat{\mathbf{B}} \;=\; \underbrace{\left\{\boldsymbol{\Phi}^{\hat{l}_m,\hat{a}_s},\ \boldsymbol{\Phi}^{\hat{l}_m,n}\right\}}_{\text{edge functions}} \;\cup\; \underbrace{\left\{\boldsymbol{\Phi}^{\hat{K},\hat{l}_m,n}, \boldsymbol{\Phi}^{\hat{K},n_1,n_2}_{(1)},\ \boldsymbol{\Phi}^{\hat{K},n_1,n_2}_{(2)}\right\}}_{\text{internal functions}},$$

where $\hat{l}_m$ are edges of $\hat{K}$, $\hat{a}_s$ are vertices of $\hat{l}_m$, n, n_1 and n_2 determine the degree of the shape functions, and the subscripts $(i), i = 1, 2$, indicate two linearly independent vector fields $\hat{\mathbf{v}}_{(i)}$ used in the definition of internal functions. Therefore, the direct decomposition $\hat{\mathbf{V}} = \hat{\mathbf{V}}^{\partial} \oplus \mathring{\hat{\mathbf{V}}}$ is naturally identified for these vector spaces, where $\mathring{\hat{\mathbf{V}}}$ is the space spanned by the internal shape functions, and $\mathbf{V}^{\partial}$ being its complement, spanned by edge (or face) shape functions.

Usually, for stability, the divergence space is $\nabla \cdot \hat{\mathbf{V}} = \hat{U} = \hat{U}_0 \oplus \hat{U}^{\perp}$, where $\hat{U}_0$ are the constant functions, and $\hat{U}^{\perp}$ is the complement formed by those functions in $\hat{U}$ with zero mean, the image of the internal functions $\mathring{\mathbf{V}}$ by the divergence operator, $\hat{U}^{\perp} = \nabla \cdot \mathring{\hat{\mathbf{V}}}$.

We also refer to [14], for the construction of such stable approximation spaces, and for their application to mixed methods for curvilinear two dimensional meshes on manifolds, to [6] for the treatment of cases based tetrahedral, affine hexahedral and affine prismatic elements, and to [15], for the assembly of them for three dimensional curved and hp-adapted meshes.

3 The mixed finite element formulation

Consider the model problem

$$\nabla \cdot \boldsymbol{\sigma} = f \quad \text{in} \quad \Omega, \tag{3}$$

$$\boldsymbol{\sigma} = -\mathcal{K}\nabla u \tag{4}$$

$$u = u_D \quad \text{in} \quad \partial\Omega, \tag{5}$$

where $f \in L^2(\Omega)$, and $u_D \in H^{1/2}(\partial\Omega)$ is the Dirichlet boundary condition. The tensor $\mathcal{K}$ is assumed to be a symmetric positive-definite matrix, composed by functions in $L^{\infty}(\Omega)$.

Given approximation spaces $\mathbf{V}_h \subset \mathbf{H}(\text{div}, \Omega)$, for the variable $\boldsymbol{\sigma}$, and $U_h \subset L^2(\Omega)$, for the variable u, as described in the previous section, consider the discrete variational mixed formulation for problem (3)-(5) [1]:
Find $(\boldsymbol{\sigma}_h, u_h) \in (\mathbf{V}_h \times U_h)$, such that $\forall \mathbf{q} \in \mathbf{V}_h$, and $\forall \varphi \in U_h$

$$a(\boldsymbol{\sigma}_h, \mathbf{q}) - b(u_h, \mathbf{q}) = - < u_D, \mathbf{q} \cdot \boldsymbol{\eta} >, \tag{6}$$

$$b(\varphi, \nabla \cdot \boldsymbol{\sigma}_h) = f(\varphi), \tag{7}$$

where $\boldsymbol{\eta}$ is the outward unit normal vector on $\partial\Omega$, $< \cdot, \cdot >$ represents the duality pairing of $H^{1/2}(\partial\Omega)$ and $H^{-1/2}(\partial\Omega)$, and

$$a(\boldsymbol{\sigma}, \mathbf{q}) = \int_\Omega \mathcal{K}^{-1}\boldsymbol{\sigma} \cdot \mathbf{q}\, d\Omega, \;\; b(u, \mathbf{q}) = \int_\Omega u \nabla \cdot \mathbf{q}\, d\Omega, \;\; f(\varphi) = \int_\Omega f\varphi\, d\Omega.$$

3.1 Error analysis

The main required tools for classic error analyses for mixed finite element methods are:

1. *Projections commuting the De Rham diagram on the master element*: For sufficiently smooth vector functions in $\mathbf{H}^\alpha(\hat{K})$, $\alpha \geq 1$, assume that on the master element a bounded projection $\hat{\boldsymbol{\pi}} : \mathbf{H}^\alpha(\hat{K}) \to \hat{\mathbf{V}}$ is defined, and consider the corresponding versions on the computational elements $\boldsymbol{\pi}_K : \mathbf{H}^\alpha(K) \to \mathbf{V}(K)$ given by $\boldsymbol{\pi}_K = \mathbb{F}_K^{div} \circ \hat{\boldsymbol{\pi}} \circ [\mathbb{F}_K^{div}]^{-1}$. A global projection $\boldsymbol{\Pi}_h : \mathbf{H}^\alpha(\Omega) \to \mathbf{V}_h$ is then piecewise defined: $(\boldsymbol{\Pi}_h \mathbf{q})|_K = \boldsymbol{\pi}_K(\mathbf{q}|_K)$. Analogously, if $\hat{\lambda}$ denotes the L^2-projection on $\hat{U}$, a global projection $\Lambda_h : L^2(\Omega) \to U_h$ is piecewise defined: $(\Lambda_h \varphi)|_K = \lambda_K(\varphi|_K)$, where $\lambda_K = \mathbb{F}_K \circ \hat{\lambda} \circ \mathbb{F}_K^{-1}$. The projections $\hat{\boldsymbol{\pi}}$ and $\hat{\lambda}$ are required to verify the commutation De Rham property illustrated by next diagram:

$$\begin{array}{ccc} \mathbf{H}^\alpha(\hat{K}) & \xrightarrow{\nabla \cdot} & L^2(\hat{K}) \\ \downarrow \hat{\boldsymbol{\pi}} & & \downarrow \hat{\lambda} \\ \hat{\mathbf{V}} & \xrightarrow{\nabla \cdot} & \hat{U} \end{array}, \tag{8}$$

meaning that

$$\int_{\hat{K}} \nabla \cdot [\hat{\boldsymbol{\pi}}\mathbf{q} - \mathbf{q}]\varphi\, d\hat{K} = 0, \;\; \forall \varphi \in \hat{U}. \tag{9}$$

2. *Expressions of flux, flux divergence and potential errors in terms of projection errors for the corresponding exact solutions*: Assuming the existence of such projections $\boldsymbol{\Pi}_h$ and Λ_h on the spaces $\mathbf{V}_h$ and U_h, approximate flux, flux divergence and potential errors can be expressed in terms of projection errors for the corresponding exact solutions, as stated in [8], Theorem 6.1.

3. *Projection error estimates*: Based on such expressions, the complete error analysis for the numerical solutions of the mixed formulation requires the study of error convergence rates for the projection $\boldsymbol{\Pi}_h$ on $\mathbf{H}(\text{div})$-conforming spaces $\mathbf{V}_h$, and of Λ_h on U_h. For that, the mesh family $\mathcal{T}_h$ are required to be shape-regular and non-degenerate, as defined in [16]. The proofs make use of classic arguments using Bramble-Hilbert lemma, and are similar to the ones of Theorem 4.1 and Theorem 4.2 in [8]. The convergence rates are established in terms of the total degrees r and t of flux and scalar polynomials that can be represented on the geometric elements K after the transformations $\mathbb{F}_K^{div}$ and $\mathbb{F}_K$ are applied to the vector

and scalar polynomial spaces $\hat{\mathbf{V}}$ and $\hat{U}$ defined on the master element, and the total degree r of scalar polynomials contained in the range of the divergence operator applied to $\hat{\mathbf{V}}$.

4. *Optimal conditions determining the orders of accuracy of the projection errors*: The parameters determining the projection convergence rates can be easily obtained when affine elements are used, since for them the actions of the function transformations $\mathbb{F}_K^{div}$ and $\mathbb{F}_K$ preserve polynomial fields. For non-affine geometric transformations, with non-constant Jacobian determinants, this is a more subtle task, specially concerning the Piola transformation. For that, some optimality concepts are required.

The error analysis for the approximate solutions is then a combination of the mentioned estimates, as stated in the following theorem.

Theorem 3.1 *Consider approximation space configurations $\{\mathbf{V}_h,\ U_h\}$, based on shape-regular and non-degenerate meshes $\mathcal{T}_h$ of a convex domain Ω, for which projections $\mathbf{\Pi}_h$ and Λ_h are defined, as discussed previously. Let s, r and t be the degree of polynomial spaces such that: (i) $[\mathbb{P}_s]^3 \subset \mathbf{V}(K)$, (ii) $\mathbb{P}_r \subset \nabla \cdot \mathbf{V}(K)$, and (iii) $\mathbb{P}_t \subset U(K)$. If $\boldsymbol{\sigma}_h \in \mathbf{V}_h$ and $u_h \in U_h$ satisfy (6)-(7), and u is regular enough, then the following estimates hold:*

$$||\boldsymbol{\sigma} - \boldsymbol{\sigma}_h||_{\mathbf{L}^2(\Omega)} \lesssim h^{s+1}||\boldsymbol{\sigma}||_{\mathbf{H}^{s+1}(\Omega)}, \tag{10}$$

$$|\nabla \cdot (\boldsymbol{\sigma} - \boldsymbol{\sigma}_h)||_{L^2(\Omega)} \lesssim h^{r+1}\ ||\nabla \cdot \boldsymbol{\sigma}||_{H^{r+1}}, \tag{11}$$

$$||u - u_h||_{L^2(\Omega)} \lesssim h^{q+1}||u||_{H^{q+1}}, \tag{12}$$

where $q = \min\{s+1, r+2, t\}$.

The estimates (10) for the flux, and (11) for the flux divergence are derived directly from their expressions in terms of projection errors, and from the corresponding projection error estimates. For the potential variable, the order of accuracy follows from similar arguments as in the proof of Theorem 6.2 in [8], and from the projection error estimates. The convexity of Ω only plays a role for the elliptic regularity property, used to get (12).

In the literature, most of the convergence estimates for the mixed method assume affine (or curved but asymtoptically affine) geometries, for which the optimal parameters s, r and t indicated in Theorem 3.1 are easily determined. In the seminal thesis by Thomas [17], curved quadrilateral meshes $\mathcal{T}_h$ are indeed considered, but they are obtained from regular affine meshes $\hat{\mathcal{T}}_h$ of a reference domain $\hat{\Omega}$, which is globally mapped by a smooth (at least C^2) invertible map $F : \mathbb{R}^2 \to \mathbb{R}^2$, such $F(\hat{\Omega}) = \Omega$, and $F(\hat{\mathcal{T}}_h) = \mathcal{T}_h$. The convergence rates for curved meshes are then obtained in terms of the corresponding ones associated to a transformed problem on the reference domain $\hat{\Omega}$, which is mapped by F from the original problem in Ω. The same hypotheses are assumed in [18] for the expanded mixed formulation proposed there.

In the above mentioned curved mesh circumstances, accuracy degradations are not observed, the same orders as for affine mesh contexts being kept. A

case for which they indeed occur has been analyzed in [8] for RT_k spaces based on non-affine quadrilateral meshes, for which the rate of divergence errors is reduced. To overcome this drawback, and adopting bilinear geometric transformations $F_K : \mathbb{R}^2 \to \mathbb{R}^2$, which are independent of the mesh resolution, and may vary for different quadrilateral elements on the partition $\mathcal{T}_h$, necessary and sufficient conditions are determined in [8] to obtain optimal error estimates for $\mathbf{H}(\text{div})$-conforming approximations based on these general quadrilateral meshes. Then, ABF_k elements are introduced to accomplich such properties, which are obtained by enriching the RT_k elements. The conclusion is that the divergence error, which may reduce to order k for the original RT_k space based on such non-affine quadrilaterals, can be improved by ABF_k approximations to the same order $k+1$ of flux and potential variables. The study in [19] also obtain the same divergence improvement using spaces called AC_k, of minimal dimension, for non-affine quadrilaterals. The error analysis in [9] is for the enriched version RT_k^+ based on this kind of non-affine quadrilaterals, which also gives order $k+1$ for the flux divergence, but with a bonus enhancement of the potential variable to order $k+2$.

3.2 Characterization of optimal spaces

Having in mind the hypotheses required by the error estimations given in Theorem 3.1, and for the determination of the projection convergence rates in the presence of non-affine bi-linear or tri-linear transformations, with non-constant Jacobian determinants, the following optimality concepts are helpful for the error analysis presented in the next sections:

- Definition A: $\hat{\mathbf{E}}_s,\ s \geq 1$, is the space of minimal dimension on $\hat{K}$ such that the following property holds

$$\hat{\mathbf{V}} \supset \hat{\mathbf{E}}_s \Longleftrightarrow \mathbf{V}(K) = \mathbb{F}_K^{div}\hat{\mathbf{V}} \supset [\mathbb{P}_{s-1}]^3. \tag{13}$$

- Definition B: $\hat{F}_r,\ r \geq 1$, is the space of minimal dimension on $\hat{K}$ such that the following property holds

$$\nabla \cdot \hat{\mathbf{V}} \supset \hat{F}_r \Longleftrightarrow \nabla \cdot \mathbf{V}(K) = \nabla \cdot \mathbb{F}_K^{div}\hat{\mathbf{V}} \supset \mathbb{P}_{r-1}. \tag{14}$$

As already mentioned, the characterization of the optimal spaces $\hat{\mathbf{E}}_s$ and $\hat{F}_r$ has been established in [8] for quadrilateral elements mapped by bi-linear mappings. The lowest order case $s = r = 1$ for curvilinear cubic meshes has been studied in [16]. For higher order cases, the characterization of the optimal spaces $\hat{\mathbf{E}}_s$ and $\hat{\mathbf{F}}_r$ has been determined in [5], Theorem 1, for general hexahedra and prisms (and also pyramids), according to the formulae bellow. We also refer to [20] for approximation properties of general differential forms on curvilinear cubic elements, using exterior calculus, the case of $\mathbf{H}(\text{div})$ d-dimensional being the particular case of $d-1$ forms.

Optimal spaces for hexahedral elements According to [5], Theorem 1, for general non-affine tri-linear transformations applied to $\hat{K} = \mathcal{H}_e$, the optimal vector spaces $\hat{\mathbf{E}}_s^{\mathcal{H}_e}$, $s > 1$, are

$$\begin{aligned}
\hat{\mathbf{E}}_s^{\mathcal{H}_e} &= \mathbb{Q}_{s+1,s-1,s-1} \times \mathbb{Q}_{s-1,s+1,s-1} \times \mathbb{Q}_{s-1,s-1,s+1} \\
&\oplus \left\{ \begin{bmatrix} \hat{x}^i \hat{y}^s \hat{z}^j \\ 0 \\ 0 \end{bmatrix} \oplus \begin{bmatrix} 0 \\ \hat{x}^j \hat{y}^i \hat{z}^s \\ 0 \end{bmatrix} \oplus \begin{bmatrix} 0 \\ 0 \\ \hat{x}^s \hat{y}^j \hat{z}^i \end{bmatrix} \quad \begin{matrix} 0 \le i \le s \\ 0 \le j \le s-1 \end{matrix} \right\} \\
&\oplus \left\{ \begin{bmatrix} \hat{x}^i \hat{y}^j \hat{z}^s \\ 0 \\ 0 \end{bmatrix} \oplus \begin{bmatrix} 0 \\ \hat{x}^s \hat{y}^i \hat{z}^j \\ 0 \end{bmatrix} \oplus \begin{bmatrix} 0 \\ 0 \\ \hat{x}^j \hat{y}^s \hat{z}^i \end{bmatrix} \quad \begin{matrix} 0 \le i \le s \\ 0 \le j \le s-1 \end{matrix} \right\} \\
&\oplus \left\{ \begin{bmatrix} \hat{x}^{s+1} \hat{y}^j \hat{z}^s \\ 0 \\ -\hat{x}^s \hat{y}^j \hat{z}^{s+1} \end{bmatrix} \oplus \begin{bmatrix} 0 \\ \hat{x}^j \hat{y}^{s+1} \hat{z}^s \\ -\hat{x}^j \hat{y}^s \hat{z}^{s+1} \end{bmatrix} \oplus \begin{bmatrix} \hat{x}^{s+1} \hat{y}^s \hat{z}^j \\ -\hat{x}^s \hat{y}^{s+1} \hat{z}^j \\ 0 \end{bmatrix} \quad 0 \le j \le s-1 \right\} \\
&= (a) \oplus (b) \oplus (c) \oplus (d). \qquad (15)
\end{aligned}$$

Furthermore, according to Proposition 1 in [5], $\hat{F}_r^{\mathcal{H}_e} = \nabla \cdot \hat{\mathbf{E}}_{r+1}^{\mathcal{H}_e}$.

Optimal elements for Prismatic elements By [5], Theorem 1, for general non-affine bi-linear transformations applied to the prism $\hat{K} = \mathcal{P}_r$, the vector optimal spaces $\hat{\mathbf{E}}_s^{\mathcal{P}_r}$ are

$$\begin{aligned}
\hat{\mathbf{E}}_s^{\mathcal{P}_r} = &\Big(\mathbb{W}_{s-1,s}(\hat{x},\hat{y},\hat{z}) \oplus \tilde{\mathbb{P}}_s(\hat{x},\hat{y}) \mathbb{P}_{s-1}(\hat{z}) \Big)^2 \times \Big(\mathbb{W}_{s-2,s+1}(\hat{x},\hat{y},\hat{z}) \oplus \tilde{\mathbb{P}}_{s-1}(\hat{x},\hat{y}) \mathbb{P}_s(\hat{z}) \Big) \\
&\oplus \tilde{\mathbb{P}}_{s-1}(\hat{x},\hat{y}) \hat{z}^s \begin{bmatrix} -\hat{x} \\ -\hat{y} \\ \hat{z} \end{bmatrix} \\
&= (a) \oplus (b), \qquad (16)
\end{aligned}$$

where $\tilde{\mathbb{P}}_s(\hat{x},\hat{y}) = x^i y^j, i + j = s$, are homogeneous polynomials. By Proposition 1 in [5], $\nabla \cdot \hat{\mathbf{E}}_s^{\mathcal{P}_r} = \mathbb{W}_{s-2,s}(\hat{x},\hat{y},\hat{z}) \oplus \tilde{\mathbb{P}}_{s-1}(\hat{x},\hat{y}) \mathbb{P}_s(\hat{z}) \subsetneqq \mathbb{W}_{s,s}$. Theorem 3, in [5] proves that $\hat{F}_r^{\mathcal{P}_r} = \mathbb{W}_{r,r}(\hat{x},\hat{y},\hat{z}) \oplus \mathbb{P}_{r-1}(\hat{x},\hat{y}) \hat{z}^{r+1} \subset \mathbb{W}_{r+1,r+1}$.

4 Approximation space configurations of type $\{\hat{\mathbf{V}}_k^{n+},\ \hat{U}_k^{n+}\}$, $n \ge 1$

Suppose that certain vector and scalar polynomial spaces $\hat{\mathbf{V}}_k$ and $\hat{U}_k$ are defined on the master element $\hat{K}$, following the general script discussed in Section 2. Namely, $\nabla \cdot \hat{\mathbf{V}}_k = \hat{U}_k$, and $\hat{\mathbf{V}}_k = \hat{\mathbf{V}}_k^{\partial} \oplus \mathring{\hat{\mathbf{V}}}_k$ is defined in terms of face and internal flux functions, the index k corresponding to the degree of face shape functions (polynomial degrees in $\mathring{\hat{\mathbf{V}}}_k$ and U_k may be different from k). Accordingly, a hierarchy of vector-valued basis $\mathbf{B}_k^{\hat{K}}$ are provided for $\hat{\mathbf{V}}_k$, which can be either of interior or of face types.

This section summarizes a general methodology for the construction of enriched space configurations of type $\{\hat{\mathbf{V}}_k^{n+},\ \hat{U}_k^{n+}\}$, $n \geq 1$, and the error estimates for the mixed method based on them. This methodology has been stated in [7] having in mind applications to two-dimensional problems, but it applies to more general contexts, without restrictions to element dimension and geometry.

The principle in the definition of vector-valued spaces for flux approximations of type $\hat{\mathbf{V}}_k^{n+}$ is to construct on the master element $\hat{K}$ vector spaces $\hat{\mathbf{V}}_k^{n+}$ formed by adding to the vector polynomials in $\hat{\mathbf{V}}_k$ those ones in $\hat{\mathbf{V}}_{k+n}$ of internal type whose divergence are in U_{k+n}. Accordingly, the scalar approximation space for the potential is formed by taking $\hat{U}_k^n = U_{k+n}$. In summary, if

$$\hat{\mathbf{V}}_k = \hat{\mathbf{V}}_k^{\partial} \oplus \mathring{\hat{\mathbf{V}}}_k,$$

then the direct decomposition for the enriched configurations are

$$\hat{\mathbf{V}}_k^{n+} = \hat{\mathbf{V}}_k^{\partial} \oplus \mathring{\hat{\mathbf{V}}}_{k+n}.$$

Thus, by construction, this kind of space configuration verify the compatibility property (1), and the mixed formulation based on it is stable.

Projections Suppose that for the original vector polynomial spaces $\hat{\mathbf{V}}_k$ the following properties hold:

1. Bounded projections $\hat{\boldsymbol{\pi}}_k : \mathbf{H}^{\alpha}(\hat{K}) \to \hat{\mathbf{V}}_k$ and $\hat{\lambda}_k : L^2(\hat{K}) \to \hat{U}_k$ verifying the commutative De Rham property are available.

2. The projections $\hat{\boldsymbol{\pi}}_k$ can be factorized as $\hat{\boldsymbol{\pi}}_k \hat{\mathbf{q}} = \hat{\boldsymbol{\pi}}_k^{\partial} \hat{\mathbf{q}} + \mathring{\hat{\boldsymbol{\pi}}}_k \hat{\mathbf{q}}$, in terms of edge and internal contributions.

Consequently, as suggested in [21] (see details in [7]), projections $\hat{\boldsymbol{\pi}}_k^{n+} : \mathbf{H}^{\alpha}(\hat{K}) \to \hat{\mathbf{V}}_k^{n+}$ are then defined as $\hat{\boldsymbol{\pi}}_k^{n+} \mathbf{q} = \hat{\boldsymbol{\pi}}_k^{n+,\partial} \hat{\mathbf{q}} + \mathring{\hat{\boldsymbol{\pi}}}_k^{n+} \hat{\mathbf{q}}$, where:

1. The edge component $\hat{\boldsymbol{\pi}}_k^{n+,\partial} \hat{\mathbf{q}} = \hat{\mathbf{q}}^{\partial} \in \hat{\mathbf{V}}^{\partial}$ is determined by

$$\int_{\partial \hat{K}} [\mathbf{q} - \hat{\mathbf{q}}^{\partial}] \cdot \hat{\boldsymbol{\eta}}\ \phi ds = 0,\ \forall \phi \in P_k(\partial \hat{K}), \tag{17}$$

   $P_k(\partial \hat{K})$ representing the normal traces of functions in $\hat{\mathbf{V}}_k$.

2. The internal term $\mathring{\hat{\boldsymbol{\pi}}}_k^{n+} \hat{\mathbf{q}} = \mathring{\hat{\mathbf{q}}} \in \mathring{\hat{\mathbf{V}}}_k^{n+} = \mathring{\hat{\mathbf{V}}}_{k+n}$ is taken as $\mathring{\mathbf{q}} = \mathring{\hat{\boldsymbol{\pi}}}_{k+n}(\mathbf{q} - \mathbf{q}_{\partial})$, where $\mathring{\hat{\boldsymbol{\pi}}}_{k+n}$ is the internal projection component of the original scheme at level $k+n$.

The commutative De Rham property is also valid for the projections $\hat{\boldsymbol{\pi}}_k^{n+}$ and $\hat{\lambda}_k^{n+} = \hat{\lambda}_{k+n}$ associated to the enriched space configuration $\{\hat{\mathbf{V}}_k^{n+},\ \hat{U}_k^{n+}\}$.

Optimal properties Assume also that the original space $\hat{\mathbf{V}}_k$ contains the optimal vector polynomial space $\hat{\mathbf{E}}_{s+1}$, and that the associated divergence space $\hat{U}_k$ contains the optimal scalar polynomial space $\hat{F}_{r+1}$, and $\mathbb{P}_t$ as well. Recall that these basic hypotheses imply that, on the mapped elements $K \in \mathcal{T}_h$, the local enriched spaces satisfy

$$\begin{aligned} \mathbf{V}_k^{n+}(K) &\supset [\mathbb{P}_s]^2, \\ \nabla \cdot \mathbf{V}_k^{n+}(K) &\supset \mathbb{P}_{r+n}, \\ U_k^{n+}(K) &\supset \mathbb{P}_{t+n}. \end{aligned}$$

After the insertion of these results in Theorem 3.1, the following error estimates hold for the flux, potential and divergence variables obtained by the mixed finite element formulation based on approximations spaces of type $\{\hat{\mathbf{V}}_k^{n+},\ \hat{U}_k^{n+}\}$ enriched space configurations.

Theorem 4.1 *Consider approximation space configurations $\{\mathbf{V}_h,\ U_h\}$ of type $\{\hat{\mathbf{V}}_k^{n+},\ \hat{U}_k^{n+}\}$, obtained by the enrichment procedure of an original space configuration $\{\hat{\mathbf{V}}_k,\ \hat{U}_k\}$ verifying the hypotheses of Theorem 3.1. Then, the following error estimates hold for the flux, potential and divergence variables, obtained by the mixed finite element formulation based on them:*

$$||\boldsymbol{\sigma} - \boldsymbol{\sigma}_h||_{\mathbf{L}^2(\Omega)} \lesssim h^{s+1} ||\boldsymbol{\sigma}||_{\mathbf{H}^{s+1}(\Omega)}, \tag{18}$$

$$|\nabla \cdot (\boldsymbol{\sigma} - \boldsymbol{\sigma}_h)||_{L^2(\Omega)} \lesssim h^{r+n+1}\ ||\nabla \cdot \boldsymbol{\sigma}||_{H^{r+n+1}}, \tag{19}$$

$$||u - u_h||_{L^2(\Omega)} \lesssim h^{q+1} ||u||_{H^{q+1}}, \tag{20}$$

where $q = \min\{s+1, r+n+2, t+n\}$.

5 Error analysis for enriched versions of some specific cases

In order to illustrate the proposed enrichment procedure described in the previous section, let us explore the following examples of original spaces $\{\hat{\mathbf{V}}_k,\ \hat{U}_k\}$, whose enriched versions $\{\hat{\mathbf{V}}_k^{n+},\ \hat{U}_k^{n+}\}$, $n \geq 1$, shall be analyzed and implemented.

1. Example 1: BDM_k spaces for tetrahedral meshes:
   $\hat{\mathbf{V}}_{BDM_k} = [\mathbb{P}_k]^3$, $\hat{U}_{BDM_k} = \mathbb{P}_{k-1}$.

2. Example 2: RT_k spaces for hexahedral meshes:
   $\hat{\mathbf{V}}_{RT_k} = \mathbb{Q}_{k+1,k,k} \times \mathbb{Q}_{k,k+1,k} \times \mathbb{Q}_{k,k,k+1}$, $\hat{U}_{RT_k} = \mathbb{Q}_{k,k,k}$.

3. Example 3: $\tilde{N}_k$ spaces for prismatic meshes:
   $[\mathbb{W}_{k,k}]^3 \subset \hat{\mathbf{V}}_{\tilde{N}_k} \subset [\mathbb{W}_{k+1,k+1}]^3$, $\hat{U}_{\tilde{N}_k} = \mathbb{W}_{k,k}$. This is the space configuration proposed in [6]. The face functions of $\tilde{N}_k$ are in $[\mathbb{W}_{k,k}]^3$, and the internal components are taken from $[\mathbb{W}_{k+1,k+1}]^3$, constrained by the property that their divergence are in $\mathbb{W}_{k,k}$. As verified in [6], despite the fact

that the divergence operator applied to the Nédélec space $\hat{\mathbf{V}}_{N_k}$ also covers $\mathbb{W}_{k,k}$, it does not contain all flux functions in $[\mathbb{W}_{k+1,k+1}]^3$ verifying this property. Thus, $\hat{\mathbf{V}}_{N_k} \subsetneq \hat{\mathbf{V}}_{\tilde{N}_k}$, the additional internal functions in $\hat{\mathbf{V}}_{\tilde{N}_k}$ being divergence free.

Table 1 contains the dimensions of face, internal and total functions associated to the original space $\hat{\mathbf{V}}_k$ of the three examples, and to their first enrichment setting $\hat{\mathbf{V}}_k^+$. For general super-enriched cases $\hat{\mathbf{V}}_k^{n+}$, $n > 1$, the dimensions are not shown, since, as in the case $n = 1$, they can be obtained from the dimension of face functions in $\hat{\mathbf{V}}_k$, and from the dimension of internal functions in $\hat{\mathbf{V}}_{k+n}$.

Element	Type	Face	Internal	Total
$\mathcal{T}e$	BDM_k	$2(k+1)(k+2)$	$\frac{1}{2}(k-1)(k+1)(k+2)$	$\frac{1}{2}(k+1)(k+2)(k+3)$
	BDM_k^+	$2(k+1)(k+2)$	$\frac{1}{2}k(k+2)(k+3)$	$\frac{1}{2}(k+2)[k(k+3)+4(k+1)]$
$\mathcal{H}$	RT_k	$6(k+1)^2$	$3k(k+1)^2$	$3(k+1)^2(k+2)$
	RT_k^+	$6(k+1)^2$	$3(k+1)(k+2)^2$	$3(k+1)[6+k(k+6)]$
$\mathcal{P}r$	$\tilde{N}_k$	$(k+1)(4k+5)$	$\frac{1}{2}k^2(3k+5)+7k-2$	$\frac{1}{2}k^2(3k+13)+16k+3$
	$\tilde{N}_k^+$	$(k+1)(4k+5)$	$\frac{1}{2}(k+1)^2(3k+8)+7k+5$	$\frac{1}{2}k^2(3k+22)+\frac{51}{2}k+14$

Table 1: Degrees of freedom of the original space $\hat{\mathbf{V}}_k$, for tetrahedral (BDM_k), hexahedral (RT_k), and prismatic ($\tilde{N}_k$) elements, and of the enriched version $\hat{\mathbf{V}}_k^+$.

Projections associated to these original space configurations are already known in the literature [1, 6]. For the determination of the optimal parameters associated to Example 2 and Example 3, for the considered non-affine elements, the following results shall be applied.

Lemma 5.1 *For hexahedral meshes mapped by tri-linear transformations, the optimal space $\hat{\mathbf{E}}_s^{\mathcal{H}_e}$ is contained in $\hat{\mathbf{V}}_{RT_s}$, but it does not contain $[\mathbb{Q}_{s,s,s}]^3$.*

Proof: By its definition in (15), its clear that $\hat{\mathbf{E}}_s^{\mathcal{H}_e} \subset \hat{\mathbf{V}}_{RT_s} = \mathbb{Q}_{s+1,s,s} \times \mathbb{Q}_{s,s+1,s} \times \mathbb{Q}_{s,s,s+1}$. However, the normal components of the first term (15)-(a) over the faces of the unit cube are in $\mathbb{Q}_{s-1,s-1}$. For the terms in (15-(b), (15)-(c) and (15)-(d), they are in $\mathbb{Q}_{s-1,s}$ or $\mathbb{Q}_{s,s-1}$. Thus, face vector functions with normal components of type $\mathbb{Q}_{s,s}$ are missing in $\hat{\mathbf{E}}_s^{\mathcal{H}_e}$, implying that $[\mathbb{Q}_{s,s,s}]^3 \not\subseteq \hat{\mathbf{E}}_s^{\mathcal{H}_e}$.

According to Theorem 3 in [5], the optimal spaces for the divergence are

$$\begin{aligned} \hat{F}_r^{\mathcal{H}_e} &= \mathbb{Q}_{r,r,r} \oplus \left\{\hat{x}^{r+1}\hat{y}^m\hat{z}^n, \hat{x}^m\hat{y}^{r+1}\hat{z}^n, \hat{x}^m\hat{y}^n\hat{z}^{r+1},\ 0 \le m,n \le r\right\} \\ &= \mathbb{Q}_{r+1,r,r} \oplus \mathbb{Q}_{r,r+1,r} \oplus \mathbb{Q}_{r,r,r+1}. \end{aligned}$$

Furthermore, Proposition 1 in [5] states that $\hat{F}_r^{\mathcal{H}_e} = \nabla \cdot \hat{\mathbf{E}}_{r+1}^{\mathcal{H}_e}$. □

Note that, the lowest order optimal spaces $\hat{\mathbf{E}}_1^{\mathcal{H}_e}$ and $\hat{F}_1$ correspond to the spaces denoted by $\hat{\mathbf{S}}_0$ and R_0 in [16], respectively. Since $\nabla \cdot \hat{\mathbf{V}}_{RT_1} = \mathbb{Q}_{1,1,1}$, which does not contains $\hat{F}_1^{\mathcal{H}_e}$, then $\nabla \cdot \mathbb{F}^{div}\hat{\mathbf{V}}_{RT_1}$ may not contain constants for

general tri-linear mappings F_K. Thus, as concluded in [16], it does not suffice to use RT_1 to get $O(h)$ of divergence errors on general hexahedral meshes mapped by tri-linear meshes.

Lemma 5.2 *For prismatic meshes mapped by bi-linear geometric transformations, $\hat{\mathbf{E}}_s^{\mathcal{P}_r}$ is contained in $\hat{\mathbf{V}}_{\tilde{N}_s}$, but it does not contain $[\mathbb{W}_{s,s}]^3$.*

Proof: Recall that $\hat{\mathbf{V}}_{\tilde{N}_s}$ is obtained by adding to $[\mathbb{W}_{s,s}]^3$ all the internal vector functions in $[\mathbb{W}_{s+1,s+1}]^3$ whose divergence are $\mathbb{W}_{s,s}$. By the definition in (16), its clear that $\hat{\mathbf{E}}_s^{\mathcal{P}_r} \subset [\mathbb{W}_{s+1,s+1}]^3$, and it has been proved that $\nabla \cdot \hat{\mathbf{E}}_s^{\mathcal{P}_r} \subset \mathbb{W}_{s,s}$. Concerning the normal traces of $\hat{\mathbf{E}}_s^{\mathcal{P}_r}$ over the faces of the master triangular prism $\mathcal{P}_r$, we observe that they are included in $\mathbb{P}_{s-1}$ on the triangular faces, and they are of type $\mathbb{Q}_{s,s-1}$ or $\mathbb{Q}_{s-1,s}$ on the quadrilateral faces. In fact, on the triangular faces $\hat{z} = 0$ and $\hat{z} = 1$, with normal $\pm[0,0,1]^t$, the normal trace of term in (16)-(a) is in $\mathbb{P}_{s-2}(\hat{x},\hat{y}) \oplus \tilde{\mathbb{P}}_{s-1}(\hat{x},\hat{y}) = \mathbb{P}_{s-1}(\hat{x},\hat{y})$, and of term in (16)-(b) is in $\tilde{\mathbb{P}}_{s-1}(\hat{x},\hat{y})$. On the quadrilateral face $y = 0$, with normal $(0,-1,0)^t$ the normal trace of the term (16)-(a) is in $\mathbb{Q}_{s-1,s}(\hat{x},\hat{z})$ and the normal trace of in (16)-(b) is zero. On the quadrilateral face $x = 0$, with normal $(-1,0,0)^t$ the normal trace of the term in (16)-(a) is in $\mathbb{Q}_{s-1,s}(\hat{y},\hat{z})$ and the normal trace of the term in (16)-(b) is zero. On the quadrilateral face $F = \hat{x} + \hat{y} = 1$, with normal $(1,1,0)^t$, the normal trace of the term in (16)-(a) has the form $\mathbb{W}_{s-1,s}(\hat{x},\hat{y},\hat{z})|_F$ or $\tilde{\mathbb{P}}_s(\hat{x},\hat{y})\mathbb{P}_{s-1}(\hat{z})|_F$, and the normal trace of the term in (16)-(b) is of the form $\tilde{\mathbb{P}}_s(\hat{x},\hat{y})\hat{z}^s|_F$, which are of type $\mathbb{Q}_{s,s-1}$ or $\mathbb{Q}_{s-1,s}$. Consequently, the face functions in $\hat{\mathbf{E}}_s^{\mathcal{P}_r}$ are in $[\mathbb{W}_{s,s}]^3$, the internal functions in $\hat{\mathbf{E}}_s^{\mathcal{P}_r}$ are in $[\mathbb{W}_{s+1,s+1}]^3$, with divergence in $\mathbb{W}_{s,s}$, implying that $\hat{\mathbf{E}}_s^{\mathcal{P}_r} \subset \hat{\mathbf{V}}_{\tilde{N}_s}$. But the face functions of $[\mathbb{W}_{s,s}]^3$, whose normal components on the quadrilateral faces are of type $\mathbb{Q}_{s,s}$, are missing in $\hat{\mathbf{E}}_s^{\mathcal{P}_r}$. Thus, $[\mathbb{W}_{s,s}]^3 \not\subseteq \hat{\mathbf{E}}_s^{\mathcal{P}_r}$. $\square$

Theorem 5.3 *Let $\{\hat{\mathbf{V}}_k,\ \hat{U}_k\}$ be any of the original space configurations associated to the three examples above. Their corresponding parameters s, r and t determining their projection error estimates, stated in Theorem 3.1, are shown in Table 2, for all geometries mapped by affine transformations, for general hexahedral elements mapped by non-affine tri-linear transformations or for general triangular prisms mapped by non-affine bi-linear transformations. Consequently, the convergence orders in L^2-norms presented in Table 3 hold for flux, potential and divergence variables obtained by the mixed finite element formulation based on enriched approximations spaces of type $\{\hat{\mathbf{V}}_k^{n+},\ \hat{U}_k^{n+}\}$ associated to the three examples.*

Proof: Recall that $\hat{U}_k = \mathbb{P}_{k-1}$ for Example 1, $\hat{U}_k = \mathbb{Q}_{k,k,k} \supset \mathbb{P}_k$ for Example 2, and $\hat{U}_k = \mathbb{W}_{k,k} \supset \mathbb{P}_k$ for Example 3. Furthermore, $\hat{\mathbb{V}}_k \supset [\mathbb{P}_k]^3$, for any of the three cases. By the fact that affine transformations preserve polynomial spaces, then for all the examples based on affine geometries $s = k$, and $r = k-1$ for Example 1, and $r = k$ for Examples 2 and 3. Similarly, $t = k-1$ for Example 1, and $t = k$ for Examples 2 and 3, for any kind of the considered affine and non-affine mesh geometry.

	A		N-A
Spaces	BDM_k	RT_k and $\tilde{N}_k$	RT_k and $\tilde{N}_k$
s	k	k	$k-1$
r	$k-1$	k	$k-2$
t	$k-1$	k	k

Table 2: Parameters s, r and t determining the rates of convergence (10)-(12), stated in Theorem 3.1, for the original space configurations $\{\hat{\mathbf{V}}_k,\ \hat{U}_k\}$ of Example 1, 2 and 3, for affine (A) elements of all geometry, and non-affine (N-A) hexahedra and prisms.

		Flux		Potential		Divergence	
Element	Space	A	N-A	A	N-A	A	N-A
$\mathcal{T}_e$	BDM_k	$k+1$	-	k	-	k	-
	$BDM^+(= BDFM_{k+1})$	$k+1$	-	$k+1$	-	$k+1$	-
	BDM_k^{+n}, $n>1$	$k+1$	-	$k+2$	-	$k+n$	-
$\mathcal{H}_e$	RT_k	$k+1$	k	$k+1$	$k+1$	$k+1$	$k-1$
	${RT_k}^{n+}$	$k+1$	k	$k+2$	$k+1$	$k+n+1$	$k+n-1$
$\mathcal{P}_r$	$\tilde{N}_k$	$k+1$	k	$k+1$	$k+1$	$k+1$	$k-1$
	$\tilde{N}_k^{n+}$	$k+1$	k	$k+2$	$k+1$	$k+n+1$	$k+n-1$

Table 3: Convergence orders in L^2-norms for the solutions of mixed element formulations based on the original space configurations $\hat{\mathbf{V}}_k\ \hat{U}_k$, and on their enriched versions $\hat{\mathbf{V}}_k^{n+}\ \hat{U}_k^{n+}$, $n \geq 1$, for Example 1, 2 and 3, based on affine (A) elements of all geometry, and non-affine (N-A) hexahedra and prisms.

For non-affine hexahedra, mapped by general tri-linear transformations, $\hat{\mathbf{E}}_k^{\mathcal{H}_e} \subset \hat{\mathbf{V}}_{RT_k}$, according to Lemma 5.1. Thus, the inclusions $\mathbb{F}_K^{div}\mathbf{V}_{RT_k} \supset \mathbb{F}_K^{div}\hat{E}_k^{\mathcal{H}_e} \supset [\mathbb{P}_{k-1}]^3$ hold, implying that $s = k-1$. Since on the master element $\nabla \cdot \hat{\mathbf{V}}_{RT_k} = \mathbb{Q}_{k,k,k} \supsetneqq \hat{F}_{k-1}^{\mathcal{H}_e}$, this fact implies that $r = k-2$.

For non-affine prisms, mapped by general bi-linear transformations, Lemma 5.2 states that $\hat{E}_k^{\mathcal{P}_r} \subset \mathbf{V}_{\tilde{N}_k}$. Consequently, for flux space configurations $\hat{\mathbf{V}}_{\tilde{N}_k}^{n+}$ associated to prisms, $\mathbb{F}_K^{div}\hat{\mathbf{V}}_{\tilde{N}_k} \supset \mathbb{F}_K^{div}\hat{E}_k^{\mathcal{P}_r} \supset [\mathbb{P}_{k-1}]^3$, which corresponds to $s = k-1$. By construction, $\nabla \cdot \mathbf{V}_{\tilde{N}_k} = \mathbb{W}_{k,k} \supsetneqq \hat{F}_{k-1}^{\mathcal{P}_r}$. From the optimality condition of $\hat{F}_{k-1}^{\mathcal{P}_r}$, we obtain that $r = k-2$.

Finally, the convergence rates shown in Table 3 are obtained by the insertion in Theorem 4.1 of the parameters s, r and t displayed in Table 2. □

Remarks

1. Note that the optimal conditions for lowest order case $r = s = 1$ have been previously analysed in [16], for hexahedral meshes. In fact, it can be verified that the optimal spaces $\hat{\mathbf{E}}_1$ and $\hat{F}_1$ correspond to the ones denoted

there by $\hat{\mathbf{S}}_0$ and R_0, respectively. Therefore, the results in Theorem 8.1 in [16] can be seen as a special case of Theorem 5.3.

2. Because there are face terms in $\hat{\mathbf{E}}_{k+1}^{\mathcal{H}_e}$ with normal components of type $\mathbb{Q}_{k+1,k}$ or $\mathbb{Q}_{k,k+1}$ (see the proof of Lemma 5.1), which can not all be included in $\hat{\mathbf{V}}_{RT_k}$ (and neither in $\hat{\mathbf{V}}_{RT_k}^{n+}, n \geq 1$), the result can not be improved to get $s > k-1$ for general hexahedra. Similarly for general prisms, in order to have $s > k-1$, it would be necessary to verify that $\hat{\mathbf{E}}_{k+1}^{\mathcal{P}_r} \subset \hat{\mathbf{V}}_{\tilde{N}_k}$, which is not possible because the normal traces of $\hat{\mathbf{E}}_{k+1}^{\mathcal{P}_r}$ on quadrilateral faces have components of type $\mathbb{Q}_{k,k+1}$ or $\mathbb{Q}_{k+1,k}$ (see the proof of Lemma 5.2), a prohibited fact in $\hat{\mathbf{V}}_{\tilde{N}_k}$ (and also in $\hat{\mathbf{V}}_{\tilde{N}_k}^{n+}, n \geq 1$).

3. It has been observed in [16] that there are some restricted classes of non-affine hexahedra for which the optimal conditions for flux and flux divergence approximations of order $O(h)$ can be verified with less restrictions. For instance, according to the property in equation (2), in order to include constants in the space $\nabla \cdot \mathbf{V}(K)$, the space $\nabla \cdot \hat{\mathbf{V}}$ should contain the polynomials defined by J_K. For general tri-linear transformations the restriction is that $\nabla \cdot \hat{\mathbf{V}}$ should contain the optimal space $F_1 = \mathbb{Q}_{2,1,1} \oplus \mathbb{Q}_{1,2,1} \oplus \mathbb{Q}_{1,1,2}$. Since $\nabla \cdot \hat{\mathbf{V}}_{RT(1)} = \mathbb{Q}_{1,1,1}$ does not contains F_1, divergence errors of $O(h)$ can not be reached for general hexahedra. However, restricted to bi-linear transformations F_K, the resulting J_K does not include terms with maximum degree 2. Therefore, divergence errors of order $O(h)$ can be reached with the RT_1 space configurations based on these restricted kind of hexahedra. Note also that $O(h)$ convergence results obtained in [2] for the $MFMFE$ method assume special non-affine hexahedra obtained by the so called h^2-perturbations.

4. Note that the sub-optimal convergence orders occurring in the presence of non-affine hexahedral and prismatic elements, namely, a reduction from order $k+1$ to k in flux accuracy, and of two units in the divergence convergence rate, from order $k+1$ to $k-1$, are more severe than the ones observed in two-dimensional cases. For instance, when quadrilateral elements are mapped by general bilinear transformations, flux accuracy for RT_k spaces stays at the same order $k+1$, as for affine quadrilaterals ones, and the divergence degradation from order $k=1$ to k is just of one unit less [8].

6 Numerical verifications

In this section we present numerical results of the application of approximation space configurations discussed on the three examples of the previous section to solve a Darcy's problem by the mixed formulation, illustrating the predicted convergence rates shown in Table 3. The model problem is defined on the unit cube $\Omega = (0,1)^3$, with f and Dirichlet boundary conditions enforced in $\partial\Omega$ such

that the analytic solution is given by the formula

$$u = \frac{\pi}{2} - \tan^{-1}\left(5\left(\sqrt{(x-1.25)^2 + (y+0.25)^2 + (z+0.25)^2} - \frac{\pi}{3}\right)\right).$$

6.1 Some comments about computational implementation

For the numerical tests presented in the next section, flux approximations are obtained from hierarchical vector shape functions constructed in [6].

The assembly of the linear system of equations of the discrete mixed formulation (6)-(7) envolves the computation of integrals over each element K, which are expressed back in the master element $\hat{K}$ thanks to a change of variable, where a factor $\frac{1}{J_K(\hat{\mathbf{x}})}$ appears on the terms involving flux shape functions mapped by the Piola transformation. These integrals can not be numerically computed exactly by using Gauss integration formulae for non-affine transformations F_K. For the applications shown in this section, where enriched space configurations are used, involving high degree of scalar potential approximations, and of internal flux shape functions, based on non-affine meshes, care had been taken in the choice of the quadrature rules, without deterioration of the the order of convergence of the method. See also [5] for some comments on this matter concerning the integration of matrix elements involving the optimal $\mathbf{H}(\text{div})$ spaces used there.

In order to apply static condensation, the degrees of freedom of the flux $\boldsymbol{\sigma}$ are organized in two parts: $\mathring{\boldsymbol{\sigma}}$, and $\boldsymbol{\sigma}^{\partial}$, referring to internal and face components of $\boldsymbol{\sigma}$, respectively. For the variable u, take u_0 be formed by constant values on each element (the choice of any other degree of freedom for u corresponding to a shape function in each element with nonzero average also works), and let u_i denote the remaining degrees of freedom except u_0. Then, static condensation is applied by eliminating the degrees of freedom $\mathring{\boldsymbol{\sigma}}$, and u_i, to get a condensed system in terms of $\boldsymbol{\sigma}^{\partial}$, and u_0, of same structure and dimension of the original scheme for $\{\hat{\mathbf{V}}_k,\ \hat{U}_k\}$. The MKL/Pardiso solver has been used for the resolution of the global condensed linear systems.

For comparison, results for related H^1-conforming simulations shall be presented, using hierarchical shape function constructed in [13]. They are classified in terms of vertex, edge, face or internal types, and similar static condensation is adopted, where the condensed systems are represented only in terms of vertex, edge and face the contributions.

All these kinds of algorithms are particularly attractive if a computational environment is available offering tools for the construction of the required enriched $\mathbf{H}(\text{div})$-conforming spaces for the usual element geometry. Typically, the requirements include hierarchic high order vector and scalar shape functions, a data structure allowing the identification of face and internal shape functions of different degree orders, and procedures for shape function restraints in two or three dimensions (as the ones usually adopted in adaptive hp-strategies). This is the case of the object oriented programming environment called NeoPZ [1], used

[1] http://github.com/labmec/neopz

for the implementations of the all the proposed and compared formulations.

6.2 Results for affine meshes

Uniform hexahedral meshes are considered with spacing $2^{-\ell}$, $\ell = 1, \cdots, 4$, and the tetrahedral meshes are obtained by the subdivision of each cubic element into six tetrahedra. Similarly, the prismatic meshes are constructed by the subdivision of each hexahedral element into two prisms.

Figure 1 presents L^2-error curves for $\boldsymbol{\sigma} = -\nabla u$, $\nabla \cdot \boldsymbol{\sigma}$, and u obtained with the mixed method using approximation space configurations BDB_2^{n+}, RT_2^{n+}, and $\tilde{N}_2^{n+}$ of Examples 1, 2, and 3, versus the parameter h indicating the maximum of element diameters. For comparison, results for the H^1-conforming formulation are also shown, using continuous approximations obtained by mapping the corresponding scalar polynomial spaces $\hat{U}_2$ in the original space. Namely, they are $\mathbb{P}_1$, $\mathbb{Q}_{2,2,2}$, and $\mathbb{W}_{2,2}$, for BDB_2, RT_2, and $\tilde{N}_2$, respectively.

We can observe that the expected convergence rates for affine meshes and space configurations are verified. It should also be observed that space enrichment for the mixed formulation has practically no effect on the magnitudes of the flux, for $n > 1$. Similarly, the potential magnitude keeps almost the same after the application of the second enrichment. On the other hand, divergence accuracy improves systematically, at every enrichment step, as predicted by the theory.

Figure 1 also illustrates the gain in convergences rates of the mixed formulations in the flux variable (of order 3) when compared with the H^1-formulations using approximations mapped from the respective original potential spaces (of order 1 for $\mathcal{T}_e$, and 2 for $\mathcal{H}_e$ and $\mathcal{P}_r$). Furthermore, since the enrichment procedure also enhances the potential accuracy, the enriched mixed formulations also give better potential approximations, with higher convergence orders.

The plots in Figure 2 are for L^2-error curves for $\boldsymbol{\sigma}$ and u, in terms of the number of equations in the static condensed systems to be solved in the mixed method, with space configurations BDB_k^{2+}, RT_k^{+}, and $\tilde{N}_k^{+}$, $k = 2, 3$ and 4, based on uniform affine tetrahedra, hexahedra, and prisms, respectively. Correspondingly, results for H^1-simulations are also shown, using scalar polynomials in $\mathbb{P}_k$, $\mathbb{Q}_{k,k,k}$, and $\mathbb{W}_{k,k}$. These plots illustrate that all the methods improve their performance by increasing the degree of their polynomial spaces, despite the increasing number of degrees of freedom required for them. The known rates of convergence for H^1 formulations (of order $k+1$ for potential and k for flux variables) are one unit less than the predicted rates for these enriched mixed formulations for affine meshes ($k+2$ and $k+1$, respectively). What the plots in Figure 2 also show is that these comparisons are also favorable for the enriched mixed methods when compared as a function of the number of condensed equations to be solved, especially for hexahedral and prismatic meshes.

For instance, instead of order 2 hold by flux approximations based on affine hexahedra, only order 1 is reached when this deformed split pattern is used, the magnitude of the error being almost insensitive to space enrichment. As expected, the divergence accuracy improves systematically, at every enrichment

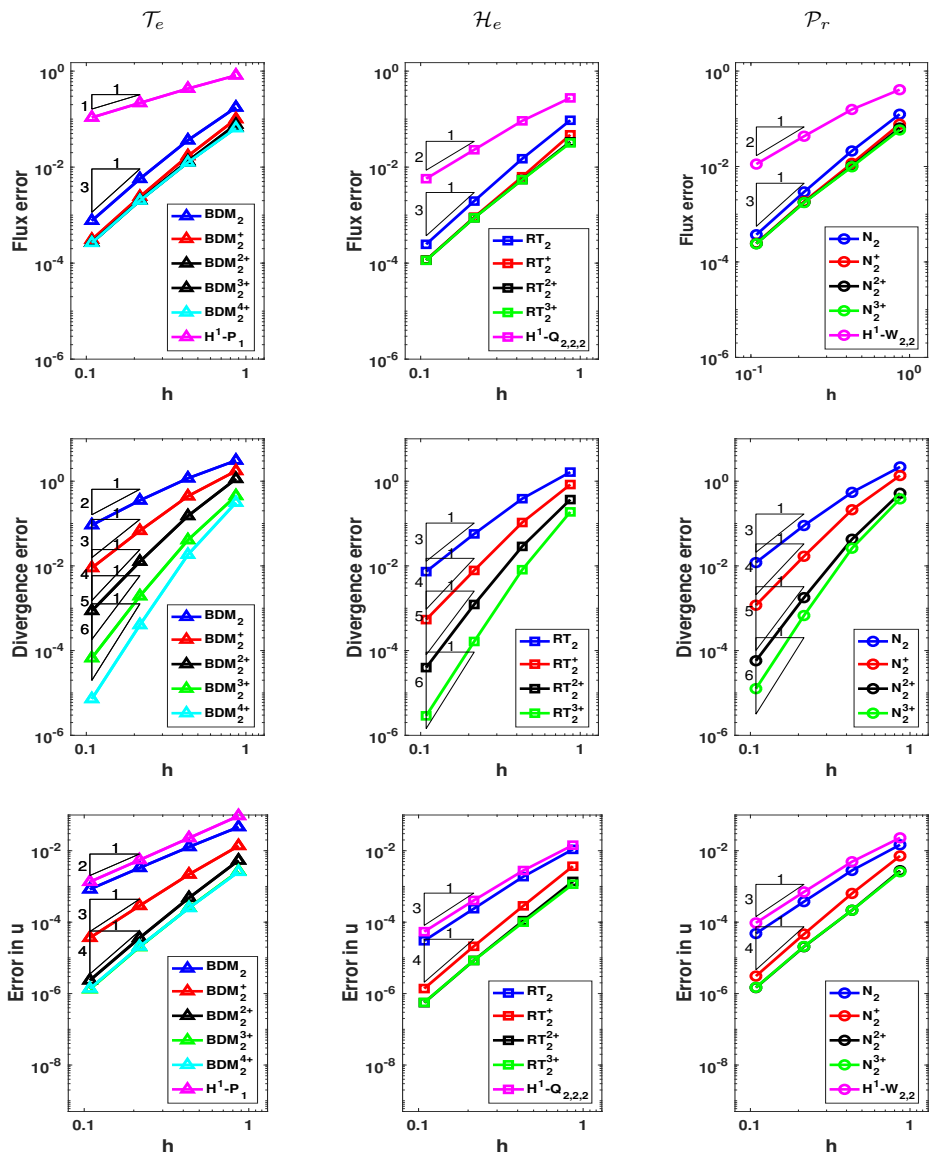

Figure 1: Affine meshes - L^2-errors for $\boldsymbol{\sigma}$, $\nabla\cdot\boldsymbol{\sigma}$, and u, versus the mesh parameter h, using the mixed formulation of Darcy's problem with space configurations BDM_2 (left column), RT_2 (midle column), and $\tilde{N}_2$ (right column), based on affine tetrahedral, hexahedral, and prismatic meshes, respectively, and their enriched versions BDB_2^{n+}, RT_2^{n+}, and $\tilde{N}_2^{n+}$. Accordingly, H^1-conforming results are based on polynomials in $\mathbb{P}_1$, $\mathbb{Q}_{2,2,2}$, and $\mathbb{W}_{2,2}$.

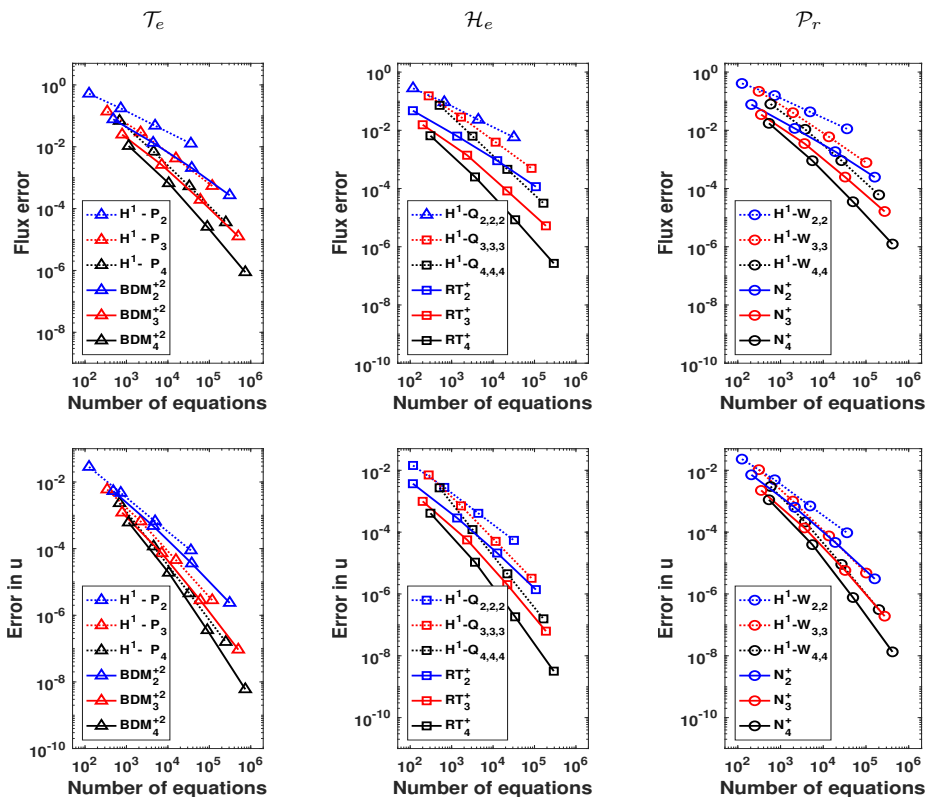

Figure 2: Affine meshes - L^2-errors for $\boldsymbol{\sigma}$ (top side) and in u (bottom side), versus the number of equations in the static condended form, using the mixed formulation of Darcy's problem with space configurations BDB_k^{2+}, RT_k^+, and $\tilde{N}_k^+$ (continuous lines), for $k = 2$ (blue) $k = 3$ (red), and $k = 4$ (black), based on affine tetrahedral (left side), hexahedral (midle side), and prismatic meshes (right side), respectively. Correspondingly, H^1-conforming results (dashed lines) are for scalar polynomials in $\mathbb{P}_k$, $\mathbb{Q}_{k,k,k}$, and $\mathbb{W}_{k,k}$.

step, but with the reduction of one unit in the convergence rates, with respect to the affine context. Concerning the error in u, the predicted order 2 is verified for any space configuration, independently or the enrichment stage. Furthermore, almost the same error magnitude is kept after the first enrichment.

6.3 Results for non-affine hexahedral meshes

For non-affine hexahedral geometry, we adopt a split pattern, as suggested in [5]. Initially, the unit cube is subdivided into 6 tetrahedra. Then, each tetrahedron is partitioned into four hexahedra. In total, 24 non-affine hexahedra are formed, composing the coarse mesh $\mathcal{T}_{h_0}$, as displayed in Figure 3 (left side). Then, on

refinement level ℓ, the same procedure is applied to all cubes of the uniform hexahedral meshes with sides $2^{-\ell}$, $\ell = 1, \cdots, 3$, to form shape regular non-affine hexahedral meshes $\mathcal{T}_{h_\ell}$, showing a constant aspect ratio 3.52586. The non-affine hexahedral mesh $\mathcal{T}_{h_1}$ is shown in Figure 3 (right side).

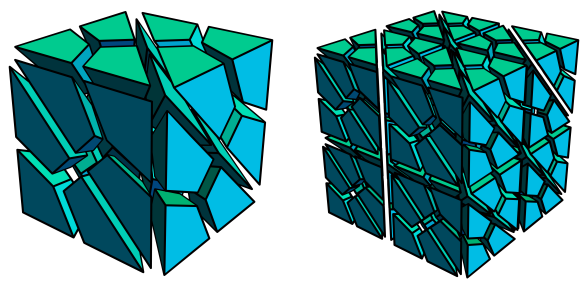

Figure 3: Illustration of the non-affine hexahedral mesh $\mathcal{T}_{h_0}$ at the coarser level (left side) and $\mathcal{T}_{h_1}$ at the next finer scale (right side).

Using the approximation space configurations RT_1, RT_1^+, and RT_1^{2+}, based on the family of non-affine hexahedral meshes, the L^2-error curves for $\boldsymbol{\sigma} = -\nabla u$, $\nabla \cdot \boldsymbol{\sigma}$, and u are displayed in the top side of Figure 4 in terms of the mesh parameter $h = h_\ell$ measuring the maximum element diameter. We can observe the deterioration of convergence rates for the flux and flux divergence, as predicted by the error analysis of the previous section.

The plots in the bottom side of Figure 4 are considered for these space configurations in terms of the number of equations to be solved. Having the same number of degrees of freedom in the static condensed form, these plots confirm the significant enhancements of the divergence and better potential resolutions when the RT_1^+, and RT_1^{2+} configurations are employed instead of the original RT_1 setting. They also show that their flux and potential error magnitudes are smaller than the corresponding ones given by the H^1 conforming formulation, even when the comparison is made in terms of the size of condensed systems to be solved.

For the readers interested in reproducing these simulations, the data corresponding to the errors plotted in Figure 3 are stored in Table 4. Corresponding results for $k = 2$ are also shown.

7 Conclusions

New insights into approximation properties of mixed finite element methods for Darcy's problems are obtained by analyzing the effect of using multi-linear mappings to form $\mathbf{H}(\mathrm{div})$-conforming spaces based on non-affine hexahedral or prismatic meshes. A reduced rate of convergence for approximations of the flux variable can be caused by the degeneration of the quadrilateral faces of the elements.

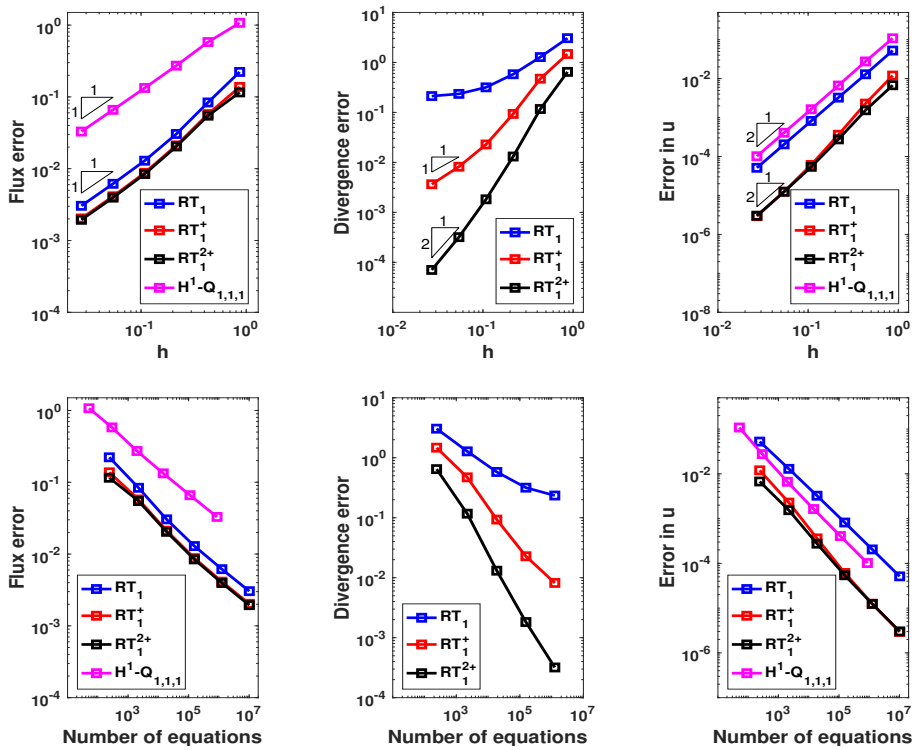

Figure 4: Non-affine split hexahedral meshes - L^2-errors in $\boldsymbol{\sigma}$, $\nabla \cdot \boldsymbol{\sigma}$, and u, versus the mesh parameter h (top side), and the number of equations in the static condended form (bottom side), using the mixed formulation of Darcy's problem based on the original RT_1 space, and on its enriched versions RT_1^+, and RT_1^{2+}. The H^1-conforming results are for the original scalar polynomial space $\mathbb{Q}_{1,1,1}$.

It is shown that the accuracy degradation observed on discretizations of the divergence operator can be attenuated by the inclusion in the flux space of some properly chosen higher degree *bubble* functions, i.e., with vanishing normal components over the master element boundary, while matching the potential scalar functions accordingly, without increasing the number of condensed equations to be solved, which corresponds to the dimension of the face flux functions. The loss of convergence in the flux variable due to quadrilateral face distortions cannot be corrected by including higher order internal functions.

The adopted enrichment methodology can be applied to general space configurations, provided some documented conditions hold, to give arbitrary high order of accuracy for the divergence operator, but without improving the rates of convergence of the approximate flux variable in L^2-norm, keeping the same rates of the original space framework. For the potential variable of enriched

schemes, accuracy improves one order only for affine meshes.

The enriched $\mathbf{H}(\text{div})$-conforming approximations have been implemented for classic space configurations based on tetrahedra, hexahedra and prisms, respectively, confirming predicted orders of convergence for affine and the kind of non-affine meshes under consideration. Numerical comparison results also show that the mixed formulation based on these enriched spaces can give more precise results for flux and potential variables than H^1-approximations, both in terms of mesh size and of the number of condensed equations to be solved. But the price to pay for extra accuracy in mixed (and also hybrid) methods is higher computational cost for matrix assembly, as shown by the comparison study in [22]. However, the effect of combining static condensation and parallelism may reduce CPU times for the mixed methods, as illustrated by an example presented in [15].

It should be remarked that if the purpose of applying the space enrichment procedure is just to restore the equilibrium of accuracy for flux and flux divergence, presumably lost by the presence of non-affine meshes, then the first space enrichment step is sufficient. However, for applications requiring better divergence accuracy and/or discretizations with higher local resolutions in multiscale mixed formulations, as in the simulation of non-linear multiphase flows, [23], the application of space configurations with increased internal orders may be convenient.

8 Acknowledgments

The authors thankfully acknowledge financial support from CNPq - Conselho Nacional de Desenvolvimento Científico e Tecnológico (the Brazilian Research Council, grants 305425/2013-7, and 304029/2013-0), and from FAPESP - Fundação de Apoio à Pesquisa do Estado de São Paulo (the Research Foundation of the State of São Paulo, Brazil, grants 2016/05144-0, 2016/05155, and 2016/13637-5). S. M. Gomes is grateful for the hospitality received during her visit to Institute Henri Poincaré, Paris, France, when part of this research has been performed.

References

[1] Franco Brezzi and Michel Fortin, *Mixed and Hybrid Finite Element Methods*, Springer Series in Computational Mathematics, vol. 15, Springer-Verlag, New York, 1991.

[2] Ross Ingram, Mary F. Weeler, and Ivan Yotov, *A Multipoint flux mixed finite element method on hexahedra*, SIAM J. Numer. Anal. 48(4) (2010):1281-1312. https://doi.org/10.1137/090766176

[3] J. C. Nédélec, *Mixed finite elements in R^3*, Numer. Math. 35 (1980):315-341.

[4] J. C. Nédélec, *A new family of mixed finite elements in* $\mathbb{R}^3$, Numer. Math. 50 (1986):57-81.

[5] Morgane Bergot and Marc Duruflé, *Approximation of* $\mathbf{H}(div)$ *with high-order optimal finite elements for pyramids, prisms and hexahedra*, Commun. Comput. Phys. 14(5)(2013):1272-1414. https://doi.org/10.4208/cicp.120712.080313a

[6] Douglas A. Castro, Philippe R. B. Devloo, Agnaldo M. Farias, Sônia M. Gomes, Denise de Siqueira, Omar Durán, *Three dimensional hierarchical mixed finite element approximations with enhanced primal variable accuracy*, Comput. Meth. Appl. Mech. Engrg. 306 (2016):479-502. https://doi.org/10.1016/j.cma.2016.03.050

[7] Philippe R. B. Devloo, Agnaldo M. Farias, Sônia M. Gomes, *A remark concerning divergence accuracy order for* $\mathbf{H}(div)$*-conforming finite element flux approximations*, arXiv:1808.03625v1 [math.NA] (2018).

[8] Douglas N. Arnold, Daniele Boffi, and Richard S. Falk, *Quadrilateral* $\mathbf{H}(div)$ *finite elements*, SIAM J, Numer. Anal. 42(6) (2005):2429-2451. https://doi.org/10.1137/S0036142903431924

[9] Agnaldo M. Farias, Philippe R. B. Devloo, Sônia M. Gomes, Denise de Siqueira, Douglas A. Castro, *Two dimensional mixed finite element approximations for elliptic problems with enhanced accuracy for the potential and flux divergence*, Comput. Math. Appl. 74(12) (2017):3283-3295. https://doi.org/10.1016/j.camwa.2017.08.013

[10] Denise de Siqueira, Philippe R. B. Devloo, Sônia M. Gomes, *A new procedure for the construction of hierarchical high order Hdiv and Hcurl finite element spaces*, Journal of Computational and Applied Mathematics, 240 (2013):204-214. https://doi.org/10.1016/j.cam.2012.09.026

[11] Franco Brezzi, Jim Douglas Jr., L. D. Marini, *Two Families of Mixed Finite Elements for Second Order Elliptic Problems*, Numer. Math. 47 (1985):217-235.

[12] Franco Brezzi, Jim Jr. Douglas, Michel Fortin, L. Donatella Marini, *Efficient rectangular mixed finite elements in two and three space variable*, ESAIM: M2AN. 21(4)(1987):581-604. https://doi.org/10.1051/m2an/1987210405811

[13] Philippe Remy Bernard Devloo, Cedric Marcelo Augusto Ayala Bravo, Edimar Cesar Rylo, *Systematic and generic construction of shape functions for p-adaptive meshes of multidimensional finite elements*, Comput. Methods Appl. Mech. Engrg. 198(21-26) (2009):1716-1725. https://doi.org/10.1016/j.cma.2008.12.022

[14] Douglas A. Castro, Philippe R. B. Devloo, Agnaldo M. Farias, Sônia M. Gomes, Omar Durán, *Hierarchical high order finite element bases for* $\mathbf{H}(div)$ *spaces based on curved meshes for two-dimensional regions or manifolds*, J. Comput. Appl. Math. 301 (2016):241-258. https://doi.org/10.1016/j.cam.2016.01.053

[15] P. R. B. Devloo, O. Durán, S. M. Gomes, N. Shauer, *Mixed finite element approximations based on 3D hp-adaptive curved meshes with two types of* $\mathbf{H}(div)$*-conforming spaces*, Int. Jr. Num. Meth. Eng. 113(7) (2017):1045-1060. https://doi.org/10.1002/nme.5698

[16] Richard S. Falk, Paolo Gatto and Peter Monk, *Hexahedral* $\mathbf{H}(div)$ *and* $\mathbf{H}(curl)$ *finite elements*, ESAIM: M2AN 45(1)(2011):115-143. https://doi.org/10.1051/m2an/2010034

[17] Jean-Marie Thomas, *Sur l'Analyse Numerique des Methodes d'Elements Finis Hybrides et Mixtes*, Thèse de Doctorat d'Etat, Université Pierre et Marie Curie, Paris, France, 1977.

[18] Todd Arbogast, Clint N. Dawson, Philip T. Keenan, Mary F. Wheeler, and Ivan Yotov, *Enhanced cell-centered finite difference for elliptic equations on general geometry*, SIAM J. Sci. Comput. 19(2) (1998):404-425. https://doi.org/10.1137/S1064827594264545

[19] Todd Arbogast and Maicon R. Correa, *Two families of H(div) mixed finite elements on quadrilaterals of minimal dimension*, SIAM J. Numer. Anal. 54(6) (2016):3332-3356. https://doi.org/10.1137/15M1013705

[20] Douglas N. Arnold, Daniele Boffi, Francesca Bonizzoni, *Finite element differential forms on curvilinear cubic meshes and their approximation properties*, Numer. Math. (2015)129:1-20. https://doi.org/10.1007/s00211-014-0631-3

[21] L. Demkowicz, P. Monk, L. Vardapetvan, W. Rachowicz, *De Rham diagram for hp finite element spaces*, Comput. Math. Appl., 39(2000):29-38. https://doi.org/10.1016/S0898-1221(00)00062-6

[22] P. R. B. Devloo, C. O. Faria, A. M. Farias, S. M. Gomes, A. F. D. Loula, S. M. C. Malta, *On continuous, discontinuous, mixed and primal hybrid finite element methods for second order elliptic problems*, International Journal for Numerical Methods in Engineering 115 (9) (2018):1081-1107. https://doi.org/10.1002/nme.5836

[23] Omar Yesid Durán Triana, *Development of a Surrogate Multiscale Reservoir Simulator Coupled with Geomechanics*, PhD Thesis, FEM-Universidade Estadual de Campinas, 2017. http://repositorio.unicamp.br/handle/REPOSIP/331516

Split hexahedral meshes														
RT_1								RT_2						
ℓ	pressure		flux		divergence			ℓ	pressure		flux		divergence	
	Error	order	Error	order	Error	order			Error	order	Error	order	Error	order
1	5.26e-2		2.23e-1		3.05e0			1	1.06e-2		7.22e-2		1.47e0	
2	1.29e-2	2.02	8.37e-2	1.41	1.28e0	1.26		2	1.74e-3	2.60	1.61e-2	2.16	4.72e-1	1.64
3	3.25e-3	1.99	3.04e-2	1.46	5.80e-1	1.14		3	2.45e-4	2.82	2.70e-3	2.58	9.33e-2	2.34
4	8.18e-4	1.99	1.29e-2	1.24	3.17e-1	0.87		4	3.14e-5	2.97	5.53e-3	2.29	2.28e-2	2.03
5	2.05e-4	2.00	6.16e-3	1.07	2.35e-1	0.44		5	3.95e-6	2.99	1.27e-4	2.12	8.18e-3	1.48
6	5.13e-5	2.00	3.04e-3	1.02	2.12e-1	0.15								

RT_1^+								RT_2^+						
ℓ	pressure		flux		divergence			ℓ	pressure		flux		divergence	
	Error	order	Error	order	Error	order			Error	order	Error	order	Error	order
1	1.19e-2		1.38e-2		1.47e0			1	2.91e-3		3.24e-2		6.47e-1	
2	2.28e-3	2.39	5.76e-2	1.26	4.72e-1	1.64		2	3.73e-4	2.96	9.04e-3	1.84	1.17e-1	2.47
3	3.62e-4	2.66	2.11e-2	1.45	9.33e-2	2.34		3	2.93e-5	3.67	1.73e-3	2.39	1.31e-2	3.16
4	6.10e-5	2.57	8.77e-3	1.27	2.28e-2	2.03		4	2.30e-6	3.67	3.59e-4	2.67	1.82e-3	2.84
5	1.25e-5	2.28	4.13e-3	1.09	8.18e-3	1.48		5	2.29e-7	3.33	8.37e-5	2.10	3.19e-4	2.51
6	2.94e-6	2.09	2.029e-3	1.02	3.65e-3	1.16								

RT_1^{2+}								RT_2^{2+}						
ℓ	pressure		flux		divergence			ℓ	pressure		flux		divergence	
	Error	order	Error	order	Error	order			Error	order	Error	order	Error	order
1	6.75e-3		1.15e-1		6.47e-1			1	1.38e-3		2.36e-2		3.27e-1	
2	1.54e-3	2.13	5.47e-2	1.08	1.17e-1	2.47		2	1.71e-4	3.01	8.31e-3	1.50	4.00e-2	3.03
3	2.75e-4	2.46	2.04e-2	1.42	1.31e-2	3.16		3	1.60e-5	3.41	1.66e-3	2.32	2.82e-3	3.83
4	5.43e-5	2.34	8.42e-3	1.27	1.82e-3	2.84		4	1.66e-6	3.27	3.49e-4	2.25	1.55e-4	4.19
5	1.24e-5	2.13	3.95e-3	1.09	3.19e-4	2.52		5	1.98e-7	3.07	8.17e-5	2.09	1.34e-5	3.53
6	3.03e-6	2.04	1.94e-3	1.03	7.05e-5	2.18								

Table 4: L^2-errors and orders of convergence for approximations of $\boldsymbol{\sigma}$, $\nabla \cdot \boldsymbol{\sigma}$, and u obtained with the mixed formulation of the Darcy's Problem, using the original space RT_1, and its enriched versions RT_1^+, and RT_1^{2+}, based on the family of split hexahedral meshes at refinement level ℓ.